

Direct calculation of the linear thermal expansion coefficients of MoS₂ via symmetry-preserving deformations

Chee Kwan Gan* and Yu Yang Fredrik Liu

Institute of High Performance Computing, 1 Fusionopolis Way, #16-16 Connexis, Singapore 138632

(Dated: 7 October 2016)

Using density-functional perturbation theory and the Grüneisen formalism, we directly calculate the linear thermal expansion coefficients (TECs) of a hexagonal bulk system MoS₂ in the crystallographic a and c directions. The TEC calculation depends critically on the evaluation of a temperature-dependent quantity $I_i(T)$, which is the integral of the product of heat capacity and $\Gamma_i(\nu)$, of frequency ν and strain type i , where $\Gamma_i(\nu)$ is the phonon density of states weighted by the Grüneisen parameters. We show that to determine the linear TECs we may use minimally two uniaxial strains in the z direction, and either the x or y direction. However, a uniaxial strain in either the x or y direction drastically reduces the symmetry of the crystal from a hexagonal one to a base-centered orthorhombic one. We propose to use an efficient and accurate symmetry-preserving biaxial strain in the xy plane to derive the same result for $\Gamma(\nu)$. We highlight that the Grüneisen parameter associated with a biaxial strain may not be the same as the average of Grüneisen parameters associated with two separate uniaxial strains in the x and y directions due to possible preservation of degeneracies of the phonon modes under a biaxial deformation. Large anisotropy of TECs is observed where the linear TEC in the c direction is about 1.8 times larger than that in the a or b direction at high temperatures. Our theoretical TEC results are compared with experiment. The symmetry-preserving approach adopted here may be applied to a broad class of two lattice-parameter systems such as hexagonal, trigonal, and tetragonal systems, which allows many complicated systems to be treated on a first-principles level.

PACS numbers: 63.20.D-, 65.40.-b, 65.40.De

Keywords: Phonon calculations, thermal properties, thermal expansion coefficients

I. INTRODUCTION

Transition-metal dichalcogenides (TMDs) TX_2 , where T is a transition metal (such as W and Mo) and X is a chalcogen (such as S, Se, and Te), receive considerable attention due to their important mechanical and electronic properties¹. Molybdenum disulfide (MoS₂), a prototypical example of TMDs, is a layered system where Mo atoms form hexagonal layers^{2,3}. Each of the Mo hexagonal layers is sandwiched between two similar lattices of S atoms, forming a trilayer^{4,5}. The atoms within each trilayer are held together by strong covalent bonds, while the trilayers of MoS₂ interact primarily through weak van der Waals interactions. It is this sandwiched structure that endows MoS₂ with the important mechanical properties for solid lubricants^{6,7}. The electronic, optical, and lattice dynamical properties have been under intense investigations^{2,3,8}. The research on multilayers of MoS₂, among many other multilayers of TMDs, has been fueled by their novel properties intrinsic to two-dimensional materials. For example, successes of MoS₂ multilayers have been demonstrated for the purposes of energy-efficient field-effect transistor⁹, advanced electrocatalysts¹⁰, thermoelectric devices^{11,12} with a large and tunable Seebeck coefficient, phototransistors¹³, superconductivity¹⁴, etc. MoS₂ is joining the ranks of other low-dimensional materials, demanding both efficient and accurate treatment of a first-principles approach^{15–18}. Even though the mechanical, electronic, and lattice dynamical properties of the equilibrium structure of MoS₂ have been studied extensively^{6,7,19}, there are relatively few first-principles

studies of the anharmonic effects²⁰ that contribute to the thermal properties such as thermal conductivity and thermal expansion coefficient (TEC).

The linear TECs of 2H-MoS₂ have been measured in Refs. 21 and 22 where it was found that the TEC along the c direction is larger than that along the a direction. On the theoretical side, TECs may be calculated by solving the vibrational self-consistent field equations²³ or the nonequilibrium Green's function method²⁴. TECs may also be determined from a quasiharmonic approximation (QHA) calculation in which a set of calculations is to be carried out over a grid or mesh of lattice-parameter points, where the dimensionality of the grid depends on the number of independent lattice parameters^{25,26}. Recently Ding and Xiao²⁷ chose six volumes to perform phonon calculations to first obtain the volumetric TEC. Another relation involving the linear TECs for a and c [Eq. 15 of Ref. [27]] was set up, and the values of TECs were solved. In this work, we develop a direct approach based on the Grüneisen formalism to calculate the TECs in the a and c directions. Our TEC results are then compared with experiment. The outline of this paper is as follows: Section II discusses the methodology used to efficiently calculate the thermal expansion coefficients of a general hexagonal system. Section III reports the results and discussion of the application of the method to MoS₂. Section IV contains the conclusions.

II. METHODOLOGY

We shall first present the expressions for TECs for a general hexagonal system obtained with the Grüneisen formalism.^{28–32} Results specific to the hexagonal MoS₂ will be presented later. The linear TECs of the crystal along the x , y and z directions, denoted by α_1 , α_2 , and α_3 , at temperature T can be described by a matrix equation

$$\begin{pmatrix} \alpha_1 \\ \alpha_2 \\ \alpha_3 \end{pmatrix} = \frac{1}{\Omega} C^{-1} \begin{pmatrix} I_1 \\ I_2 \\ I_3 \end{pmatrix} \quad (1)$$

where Ω is the equilibrium volume of the primitive cell and C^{-1} is the elastic compliance matrix³³. The values C_{ij} are the matrix elements of the elastic constant matrix C that corresponds to a hexagonal system³⁴ where

$$C = \begin{pmatrix} C_{11} & C_{12} & C_{13} \\ C_{12} & C_{11} & C_{13} \\ C_{13} & C_{13} & C_{33} \end{pmatrix} \quad (2)$$

The integrated quantities in Eq. 1 are given by

$$I_i(T) = \frac{\Omega}{(2\pi)^3} \sum_{\lambda} \int_{\text{BZ}} d\mathbf{k} \gamma_{i,\lambda\mathbf{k}} c(\nu_{\lambda\mathbf{k}}, T) \quad (3)$$

where the integral is over the first Brillouin zone (BZ). The frequency $\nu_{\lambda\mathbf{k}}$ of a phonon mode depends on the mode index λ and wavevector \mathbf{k} . The heat capacity contributed by a phonon mode with frequency ν at temperature T is $c(\nu, T) = k_B (r/\sinh r)^2$ with $r = h\nu/2k_B T$, where h and k_B are the Planck and Boltzmann constants, respectively. The Grüneisen parameter $\gamma_{i,\lambda\mathbf{k}} = -\nu_{\lambda\mathbf{k}}^{-1} \partial \nu_{\lambda\mathbf{k}} / \partial \epsilon$ measures the relative change of a phonon frequency $\nu_{\lambda\mathbf{k}}$ as a result of an i -type deformation with strain size ϵ applied to the crystal. For example, if a uniaxial strain is applied in the x direction, then the strain parameters are $(\epsilon, 0, 0, 0, 0, 0)$ (in the Voigt notation³⁴), i.e., $\epsilon_1 = \epsilon$, and $\epsilon_j = 0$, for $j = 2, \dots, 6$. We apply uniaxial strains in the x , y , and z directions to determine $I_1(T)$, $I_2(T)$, and $I_3(T)$, respectively. Grüneisen parameters are evaluated using a central-difference scheme, where a change in the dynamical matrices before and after deformation is used in the perturbation theory to deduce the changes in eigenfrequencies³².

By a proper sampling in the k -space, we may calculate the phonon density of states as

$$\rho(\nu) = \frac{\Omega}{(2\pi)^3} \sum_{\lambda} \int_{\text{BZ}} d\mathbf{k} \delta(\nu - \nu_{\lambda\mathbf{k}}) \quad (4)$$

Next we introduce a related quantity, $\Gamma_i(\nu)$, the phonon density of states weighted by the Grüneisen pa-

rameters as

$$\Gamma_i(\nu) = \frac{\Omega}{(2\pi)^3} \sum_{\lambda} \int_{\text{BZ}} d\mathbf{k} \delta(\nu - \nu_{\lambda\mathbf{k}}) \gamma_{i,\lambda\mathbf{k}} \quad (5)$$

The usefulness of $\Gamma_i(\nu)$ is that we may obtain $I_i(T)$ in Eq. 3 from another relation

$$I_i(T) = \int_{\nu_{\min}}^{\nu_{\max}} d\nu \Gamma_i(\nu) c(\nu, T) \quad (6)$$

where ν_{\min} and ν_{\max} are the minimum and maximum frequencies of all phonon modes in the BZ, respectively.

To calculate the linear TECs, it appears that a set of three uniaxial deformations in the x , y , and z directions is needed. However, due to the symmetry of the hexagonal system, we should have $\alpha_1 = \alpha_2$ on physical grounds and hence $I_1(T) = I_2(T)$, so that the TEC Eq. 1 reduces to

$$\begin{pmatrix} \alpha_1 \\ \alpha_3 \end{pmatrix} = \frac{1}{\Omega} \begin{pmatrix} [C_{11} + C_{12}] & C_{13} \\ 2C_{13} & C_{33} \end{pmatrix}^{-1} \begin{pmatrix} I_1 \\ I_3 \end{pmatrix} \quad (7)$$

or

$$\begin{pmatrix} \alpha_1 \\ \alpha_3 \end{pmatrix} = \frac{1}{\Omega D} \begin{pmatrix} C_{33} & -C_{13} \\ -2C_{13} & [C_{11} + C_{12}] \end{pmatrix} \begin{pmatrix} I_1 \\ I_3 \end{pmatrix} \quad (8)$$

where $D = (C_{11} + C_{12})C_{33} - 2C_{13}^2$. Therefore, for a hexagonal system two uniaxial strains, the first one in either the x or y direction and the second one in the z direction, are sufficient to determine the linear TECs. For MoS₂, the symmetry of the hexagonal system is not altered [the space group remains as $P6_3/mmc$ (#194)] when a uniaxial strain is applied in the z direction. However, the symmetry is significantly lowered from hexagonal with a space group of $P6_3/mmc$ (#194) to base-centered orthorhombic with a space group of $Cmcm$ (#63) after a uniaxial strain is applied in the x or y direction. This will result in an increase of the computational cost compared to that which preserves the hexagonal symmetry where a phonon calculation is to be performed. For example, after applying a uniaxial strain in the x direction, a $5 \times 5 \times 5$ q mesh required in a phonon calculation will result in 27 irreducible q points and 486 irreducible representations or 486 self-consistent field calculations. This is to be compared with the symmetry-preserving deformations (e.g., a uniaxial strain in the z direction) where the number of irreducible q points is 15 and the number of irreducible representations is 252, which clearly shows substantial computational savings. More savings are expected when complicated crystal structures are treated.

We propose to use a computationally efficient, symmetry-preserving biaxial strain in the xy plane (hereafter it shall be called an xy biaxial strain) where $\epsilon_1 = \epsilon_2 = \epsilon$ to evaluate the Grüneisen parameters $\gamma_{b,\lambda\mathbf{k}}$ and use Eq. 3 or Eq. 6 to obtain $I_b(T)$. Due to the underlying symmetry, $I_b(T) = I_1(T) = I_2(T)$. However it should be noted that Grüneisen parameters due to an xy biaxial strain may not be the same as the average of the

Grüneisen parameters due to x and y uniaxial strains. These points will be elaborated later.

The phonon spectra of MoS₂ are calculated with density functional perturbation theory (DFPT)³⁵. For the unstrained structure, a q mesh of $5 \times 5 \times 5$ is used for the phonon calculations, which is equivalent to evaluating the force constants^{36,37} using a $5 \times 5 \times 5$ supercell. The phonon calculations proceed by evaluating dynamical matrices at a number of irreducible q points. From the dynamical matrices the interatomic force constants in the real space are obtained by an inverse Fourier transform, and these force constants are used to construct dynamical matrices at any \mathbf{k} to calculate the phonon eigenfrequencies $\nu_{\lambda\mathbf{k}}$. For the strained structures, a q mesh of $5 \times 5 \times 5$ is also used. For the unstrained structure, a larger q mesh of $6 \times 6 \times 6$ is used to confirm that a q mesh of $5 \times 5 \times 5$ is sufficient for the purposes of TEC calculations.

III. RESULTS AND DISCUSSIONS

The bulk MoS₂ belongs to the $P6_3/mmc$ nonsymmorphic space group (# 194), with two inequivalent atoms, where a Mo atom occupies a $2c(1/3, 2/3, 1/4)$ site and a S atom occupies a $4f(1/3, 2/3, z)$ site, $z = 0.6213$. This gives a total of six atoms in the hexagonal primitive cell. Density-functional theory (DFT) calculations are carried out using the plane-wave basis code Quantum Espresso³⁸. The orientation of the crystal adopted in this work is dictated by the choice of the primitive lattice vectors, where $\mathbf{a}_1 = (a, 0, 0)$, $\mathbf{a}_2 = (-a/2, a\sqrt{3}/2, 0)$, and $\mathbf{a}_3 = (0, 0, c)$ and a and c are the hexagonal lattice parameters. We use 60 Ry as the cutoff energy for the plane-wave basis set. The local-density approximation (LDA) is used to describe the exchange and correlation. For MoS₂ multilayers it has been demonstrated⁵ that the calculated phonon frequencies using LDA agree well with the experimental results. However, we should point out that the van der Waals interactions may be important in the calculation of phonon dispersion relations for some layered systems such as graphite³⁹. Pseudopotentials for Mo and S are generated from pslibrary.1.0.0 based on the Rappe-Rabe-Kaxiras-Joannopoulos⁴⁰ scheme. A $13 \times 13 \times 4$ Monkhorst-Pack k -point mesh is used. The hexagonal lattice parameters and the atomic positions are fully relaxed. The force tolerance is taken to be 10^{-3} eV/Å. We obtain $a_0 = 3.125$ Å and $c_0 = 12.086$ Å, which is in good agreement with the experimental result⁴¹ of $a = 3.160$ Å, and $c = 12.294$ Å. This is also consistent with the fact that LDA tends to overbind in crystals. We perform elastic-constant calculations^{42,43} to obtain the elastic constants $(C_{11}, C_{12}, C_{13}, C_{33}, C_{44}) = (242.35, 58.84, 11.31, 51.70, 19.60)$ GPa. These results are in very good agreement with other computational results⁴⁴ where the values of $(C_{11}, C_{12}, C_{13}, C_{33}, C_{44}) = (238, 64, 12, 57, 18)$ GPa. The agreement of our results with the experimental results⁴⁵ is rather good except for C_{12} and C_{13} (where the experimental values of $C_{12} =$

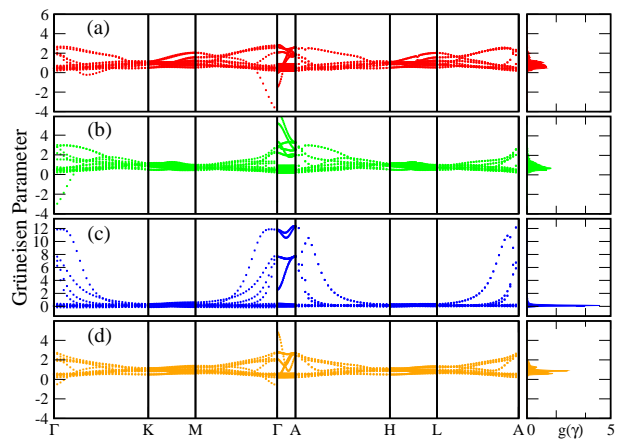


FIG. 1. (Color online) Grüneisen parameters $\gamma_{i,\lambda\mathbf{k}}$ along the high-symmetry directions for hexagonal MoS₂, for (a) x uniaxial, (b) y uniaxial, (c) z uniaxial, and (d) xy biaxial strains. The corresponding densities of Grüneisen parameters, $g_i(\gamma)$, are shown on the right. A mesh of $30 \times 30 \times 10$ for the k -point sampling is used to calculate $g_i(\gamma)$.

−54 GPa and $C_{13} = 23$ GPa), which may be due to the fact these two values are not directly determined in experiment, as discussed in Ref. [44].

We perform uniaxial deformations in the x , y , and z directions with strains set to $\epsilon = \pm 0.5\%$. For the xy biaxial deformations, $\epsilon = \pm 0.25\%$. The Grüneisen parameters $\gamma_{i,\lambda\mathbf{k}}$ along the high-symmetry directions due to these deformations are shown in Fig. 1(a)–(d). To quantify more clearly the distribution of Grüneisen parameters in the BZ, we calculate the density of Grüneisen parameters according to

$$g_i(\gamma) = \frac{\Omega}{(2\pi)^3} \sum_{\lambda} \int_{\text{BZ}} d\mathbf{k} \delta(\gamma - \gamma_{i,\lambda\mathbf{k}}) \quad (9)$$

which is shown in the right panels in Fig. 1. The density of Grüneisen parameters due to x uniaxial, y uniaxial, and xy biaxial strains are also displayed in the inset of Fig. 2(b) for a direct comparison. From Figs. 1(a) and 1(d), some negative Grüneisen parameters are observed near the Γ point, which correspond to the lowest transverse acoustic (ZA) modes. However, the plots for densities of Grüneisen parameters, $g_i(\gamma)$, show most Grüneisen parameters are populated between the small range of 0 to 2, and negative Grüneisen parameters are completely suppressed. The $g_i(\gamma)$ plots also show that large Grüneisen parameters, say, $g_i(\gamma) > 2$, are totally negligible when sampling is taken. From Fig. 1(c) we note that most Grüneisen parameters are very small for z uniaxial deformation, which is consistent with the fact that weak van der Waals interactions exist between MoS₂ trilayers.

The phonon density of states of the unstrained structure is shown in Fig. 2(a) where there is a frequency gap from 240 to 285 cm^{-1} . The density of states weighted by

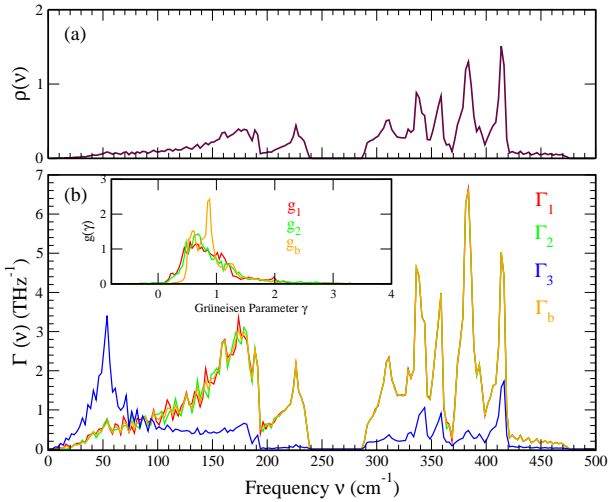


FIG. 2. (Color online) (a) The phonon density of states $\rho(\nu)$ for the unstrained MoS₂ structure. (b) The phonon density of states weighted by the Grüneisen parameters, $\Gamma_i(\nu)$. The indices $i = 1, 2, 3, b$ correspond to x uniaxial, y uniaxial, z uniaxial, and xy biaxial strains, respectively. The inset shows the densities of Grüneisen parameters, $g_i(\nu)$, for $i = 1, 2, b$.

the Grüneisen parameters, $\Gamma_i(\nu)$, is shown in Fig. 2(b), where a gap is inherited from Fig. 2(a). We note that, $\Gamma_3(\nu)$, which is due to a z uniaxial strain, has a broad peak near 50 cm^{-1} due to the fact that these frequencies are associated with more significant Grüneisen parameters [see Eq. 5]. It is interesting to see that, while the density of Grüneisen parameters due to the xy biaxial strain, $g_b(\gamma)$, is quite different from that due to the x or y uniaxial strains as shown in the inset in Fig. 2(b) (or even the average of Grüneisen parameters due to x and y uniaxial strains), $\Gamma_1(\gamma)$, $\Gamma_2(\gamma)$, and $\Gamma_b(\gamma)$ are essentially the same numerically, as shown in Fig. 2(b). This justifies the proposal to use an xy biaxial strain to replace an x uniaxial or y uniaxial strain to calculate the integrated quantity $I_b(T)$.

We now provide two pieces of evidence that explain the difference between Grüneisen parameters obtained with an xy biaxial strain and the average of Grüneisen parameters obtained with x and y uniaxial strains. Fig. 3 shows the phonon dispersions of the equilibrium structure and the strained systems along that $\Gamma - A$ path. Figs. 3(b)-(e) focus on the change in frequencies around 290 cm^{-1} . It can be seen from Figs. 3(b) and 3(e) that a xy biaxial strain cannot destroy the degeneracies of two doubly degenerate E_{2u} and E_{1g} phonon modes. However, as seen in Fig. 3(c), under an x uniaxial deformation, the two doubly degenerate E_{2u} and E_{1g} phonon modes around 290 cm^{-1} split into four nondegenerate phonon modes. Fig. 3(d) shows the same splittings for a y uniaxial strain. This explains the average of Grüneisen parameters due to x and y strains is not the same as that due to an xy biaxial strain. However, the integrations according to Eq. 5 associated with x uniaxial, y uniaxial, and xy biax-

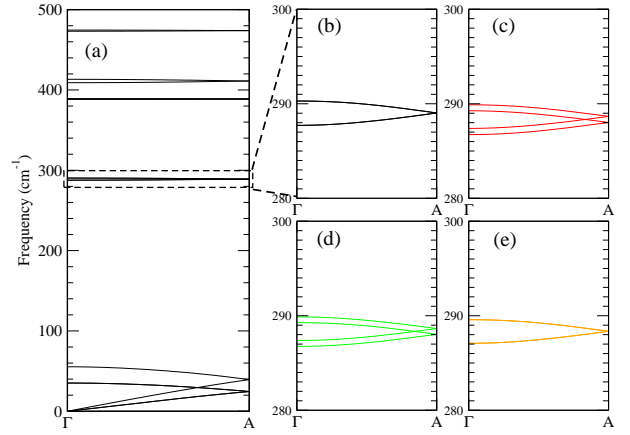


FIG. 3. (Color online) (a) The phonon dispersion of unstrained MoS₂ along the $\Gamma - A$ path. (b) Two doubly degenerate phonon modes for the unstrained structure (at Γ , the frequencies are 287.7 and 290.3 cm^{-1} for E_{2u} and E_{1g} , respectively). (c), (d), and (e) The detailed variations of the phonon frequencies for the x uniaxial, y uniaxial, and xy biaxial strained structures, respectively. The strain values for uniaxial and biaxial strains are +0.5 % and +0.25%, respectively.

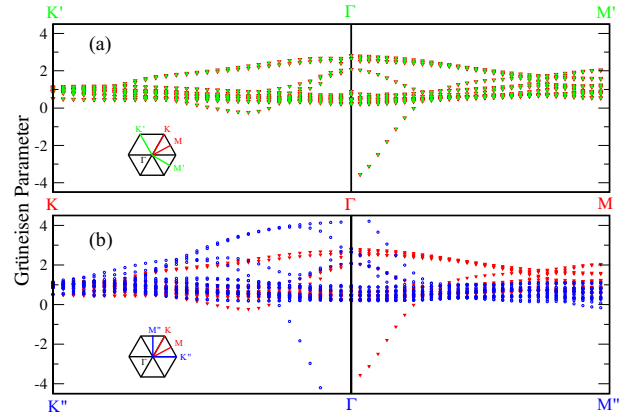


FIG. 4. (Color online) Grüneisen parameters obtained with x uniaxial strains. The chosen paths are (a) $K - \Gamma - M$ and $K' - \Gamma - M'$, and (b) $K - \Gamma - M$ and $K'' - \Gamma - M''$. The paths are shown in the insets.

ial strains give rise to the same phonon density of states weighted by the Grüneisen parameters, a fact which is expected on physical ground.

Fig. 4 furnishes another piece of evidence that under an x uniaxial strain, the planar BZ now has a fourfold rotation symmetry, in contrast to the sixfold rotation symmetry for the case of biaxial strain (where the hexagonal symmetry is preserved). The agreement of Grüneisen parameters along $K - \Gamma$ and $K' - \Gamma$ paths in Fig. 4(a) shows that there is a reflection symmetry around the y axis. Similarly, the agreement of Grüneisen parameters between those along the $\Gamma - M$ and $\Gamma - M'$ paths shows that there is a reflection symmetry around the x axis. Under the sixfold rotation symmetry of the planar BZ,

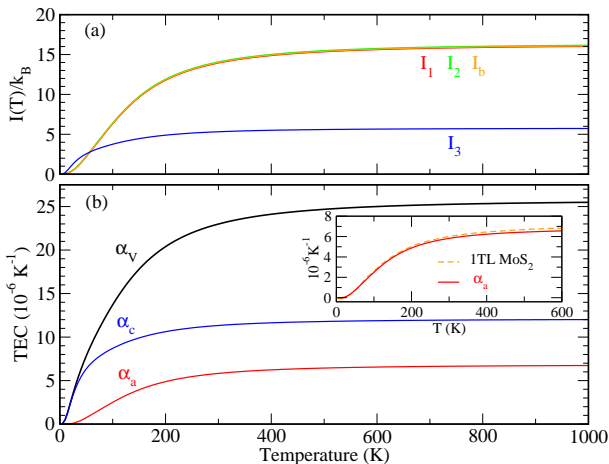


FIG. 5. (Color online) (a) The integrated quantities $I_i(T)$ as a function of temperature. (b) The linear TECs of MoS₂ along the a and c directions denoted by α_a and α_c , respectively, as a function of temperature. The volumetric TEC is denoted by α_v . The insert shows the comparison of α_a with the in-plane TEC of a single-trilayer MoS₂, obtained using a QHA approach¹⁸.

we expect Grüneisen parameters to be the same along the $K - \Gamma$ and $K'' - \Gamma$ paths, or along the $\Gamma - M$ and $\Gamma - M''$ paths. However, Fig. 4(b) shows that there is no agreement of Grüneisen parameters along the $K - \Gamma$ and $K'' - \Gamma$ paths, or along the $\Gamma - M$ and $\Gamma - M''$ paths.

The integrated quantities $I_1(T)$, $I_2(T)$, and $I_b(T)$ shown in Fig. 5(a) are essentially identical, and they are much larger than I_3 , which is due to a z uniaxial strain. This may be traced to the fact that interactions between MoS₂ trilayers are weak compared to in-plane interactions that result in smaller Grüneisen parameters (i.e., smaller frequency changes) for z strains. The linear TECs in the a and c directions are shown in Fig. 5(b). Even though $I_3(T)$ is about three times smaller than $I_b(T)$ for, say, $T > 400$ K, $\alpha_c(T)$ is larger than $\alpha_a(T)$. At $T = 1000$ K, $\alpha_a = 6.73 \times 10^{-6} \text{K}^{-1}$, $\alpha_c = 12.01 \times 10^{-6} \text{K}^{-1}$, and the volumetric TEC $\alpha_v = 2\alpha_a + \alpha_c = 25.47 \times 10^{-6} \text{K}^{-1}$. The main reason for this is that the value of C_{33} (51.70 GPa) is much smaller than the value of $C_{11} + C_{12}$ (301.19 GPa); therefore, according to Eq. 7, it is possible that α_c is larger than α_a . The result that α_c is indeed larger than α_a is consistent with the physical fact that it is easier to perform a deformation in the z direction than in the in-plane direction, which is again, attributed to the weak interactions in the out-of-plane direction. This is also confirmed by the results shown in the inset of Fig. 5(b) where there is a striking similarity between the temperature dependences of in-plane TECs for both the bulk MoS₂ and a single-trilayer MoS₂, which is obtained from a QHA-LDA treatment¹⁸. El-Mahalawy and Evans²¹ measured the linear TECs of 2H-MoS₂ between 293 and 1073 K and reported $\alpha_a = 1.9 \times 10^{-6} \text{K}^{-1}$ and $\alpha_c = 8.65 \times 10^{-6} \text{K}^{-1}$, which are con-

sistently lower than our values. The same group²² again measured the TECs of 2H-MoS₂ between 10 and 320 K and found a larger $\alpha_a = 4.922 \times 10^{-6} \text{K}^{-1}$, which agrees better with our result, and $\alpha_c = 18.580 \times 10^{-6} \text{K}^{-1}$, which is somewhat larger. We find the behavior of the rate of change of α_c with T to be different from that of α_a , where the former increases rapidly at low T while the latter increases more gradually with T . Murray and Evans²² have pointed out that the lattice constant a (c) increases linearly (nonlinearly) with temperature, which is consistent with our TEC results at low T .

IV. CONCLUSIONS

In summary, we have proposed a direct way to calculate the linear thermal expansion coefficients (TECs) of a hexagonal system based on the Grüneisen formalism. We have also proposed a way to replace the inefficient symmetry-lowering uniaxial strains by the efficient symmetry-preserving biaxial strains. We successfully implemented the computational schemes and applied them to a technologically important material, MoS₂. We found that MoS₂ has a large TEC anisotropy where the thermal expansion coefficient in the c direction is 1.8 times larger than that in the a direction at high temperatures. We highlighted that even though the integrated quantities $I_i(T)$ required by the TEC calculations can be obtained via a symmetry-preserving biaxial strain, the Grüneisen parameters from a biaxial strain may not be a simple average of the Grüneisen parameters from uniaxial x and y strains. We demonstrated that we only need a minimum of two symmetry-preserving deformations to directly calculate the TECs of a general hexagonal system. In contrast, the quasiharmonic approximation, when dealing with a two-parameter system, may require an expensive search in the two-dimensional search space. Therefore, we expect that the strategies adopted in this paper to treat a general two-lattice-parameter hexagonal system can be similarly applied to treat other two lattice-parameter systems such as trigonal and tetragonal systems, thus opening the door for a truly predictive TEC calculation for many important materials. We also expect the TEC calculations based on the Grüneisen formalism via symmetry-preserving deformations may be readily incorporated in any phonon related codes such as PHONOPY⁴⁶.

ACKNOWLEDGMENTS

We acknowledge stimulating and fruitful discussions with Ching Hua Lee. We thank the National Supercomputing Center, Singapore, for computing resources. Y.Y.F.L. acknowledges support from the Singapore National Science Scholarship.

- * Corresponding author: ganck@ihpc.a-star.edu.sg
- ¹ J. A. Wilson and A. D. Yoffe, *Adv. Phys.* **18**, 193 (1969).
 - ² J. L. Verble and T. J. Wieting, *Phys. Rev. Lett.* **25**, 362 (1970).
 - ³ T. J. Wieting and J. L. Verble, *Phys. Rev. B* **3**, 4286 (1971).
 - ⁴ X. Zhang, W. P. Han, J. B. Wu, S. Milana, Y. Lu, Q. Q. Li, A. C. Ferrari, and P. H. Tan, *Phys. Rev. B* **87**, 115413 (2013).
 - ⁵ Y. Zhao, X. Luo, H. Li, J. Zhang, P. T. Araujo, C. K. Gan, J. Wu, H. Zhang, S. Y. Quek, M. S. Dresselhaus, et al., *Nano Lett.* **13**, 1007 (2013).
 - ⁶ R. Aksoy, Y. Ma, E. Selvi, M. C. Chyu, A. Ertas, and A. White, *J. Phys. Chem. Solids* **67**, 1914 (2006).
 - ⁷ C. Lee, Q. Li, W. Kalb, X.-Z. Liu, H. Berger, R. W. Carpick, and J. Hone, *Science* **328**, 76 (2010).
 - ⁸ S. V. Bhatt, M. P. Deshpande, V. Sathe, R. Raoc, and S. H. Chakia, *J. Raman Spec.* **45**, 971 (2014).
 - ⁹ B. Radisavljevic, A. Radenovic, J. Brivio, i. V. Giacometti, and A. Kis, *Nat. Nanotechnol.* **6**, 147 (2011).
 - ¹⁰ Y. Li, H. Wang, L. Xie, Y. Liang, G. Hong, and H. Dai, *J. Am. Chem. Soc.* **133**, 7296 (2011).
 - ¹¹ M. Buscema, M. Barkelid, V. Zwiller, H. S. van der Zant, G. A. Steele, and A. Castellanos-Gomez, *Nano Lett.* **13**, 358 (2013).
 - ¹² W. Huang, X. Luo, C. K. Gan, S. Y. Quek, and G. Liang, *Phys. Chem. Chem. Phys.* **16**, 10866 (2014).
 - ¹³ Z. Yin, H. Li, H. Li, L. Jiang, Y. Shi, Y. Sun, G. Lu, Q. Zhang, X. Chen, and H. Zhang, *ACS Nano* **6**, 74 (2011).
 - ¹⁴ D. Costanzo, S. Jo, H. Berger, and A. F. Morpurgo, *Nat. Nanotechnol.* **11**, 339 (2016).
 - ¹⁵ A. Molina-Sánchez and L. Wirtz, *Phys. Rev. B* **84**, 155413 (2011).
 - ¹⁶ Y. Cheng, Z. Zhu, and U. Schwingenschlögl, *RSC Adv.* **2**, 7798 (2012).
 - ¹⁷ Y. Cai, J. Lan, G. Zhang, and Y.-W. Zhang, *Phys. Rev. B* **89**, 035438 (2014).
 - ¹⁸ C. Sevik, *Phys. Rev. B* **89**, 035422 (2014).
 - ¹⁹ C. Ataca, M. Topsakal, E. Aktürk, and S. Ciraci, *J. Phys. Chem. C* **115**, 16354 (2011).
 - ²⁰ J. Shiomi, K. Esfarjani, and G. Chen, *Phys. Rev. B* **84**, 104302 (2011).
 - ²¹ S. H. El-Mahalawy and B. L. Evans, *J. Appl. Cryst.* **9**, 403 (1976).
 - ²² R. Murray and B. L. Evans, *J. Appl. Cryst.* **12**, 312 (1979).
 - ²³ B. Monserrat, N. D. Drummond, and R. J. Needs, *Phys. Rev. B* **87**, 144302 (2013).
 - ²⁴ J.-W. Jiang, J.-S. Wang, and B. Li, *Phys. Rev. B* **80**, 205429 (2009).
 - ²⁵ M. Lazzeri and S. de Gironcoli, *Phys. Rev. Lett.* **81**, 2096 (1998).
 - ²⁶ N. Mounet and N. Marzari, *Phys. Rev. B* **71**, 205214 (2005).
 - ²⁷ Y. Ding and B. Xiao, *RSC Adv.* **5**, 18391 (2015).
 - ²⁸ E. Grüneisen, *Handb. Phys.* **10**, 1 (1926).
 - ²⁹ P. Pavone, K. Karch, O. Schütt, W. Windl, D. Strauch, P. Giannozzi, and S. Baroni, *Phys. Rev. B* **48**, 3156 (1993).
 - ³⁰ T. H. K. Barron, J. G. Collins, and G. K. White, *Adv. Phys.* **29**, 609 (1980).
 - ³¹ P. K. Schelling and P. Keblinski, *Phys. Rev. B* **68**, 035425 (2003).
 - ³² C. K. Gan, J. R. Soh, and Y. Liu, *Phys. Rev. B* **92**, 235202 (2015).
 - ³³ C. Kittel, *Introduction to Solid State Physics* (Wiley, New York, 1996), 7th ed.
 - ³⁴ J. F. Nye, *Physical Properties of Crystals: Their Representations by Tensors and Matrices* (Clarendon, Oxford, 1985).
 - ³⁵ S. Baroni, S. de Gironcoli, A. D. Corso, and P. Giannozzi, *Rev. Mod. Phys.* **73**, 515 (2001).
 - ³⁶ Y. Liu, K. T. E. Chua, T. C. Sum, and C. K. Gan, *Phys. Chem. Chem. Phys.* **16**, 345 (2014).
 - ³⁷ C. K. Gan, Y. P. Feng, and D. J. Srolovitz, *Phys. Rev. B* **73**, 235214 (2006).
 - ³⁸ P. Giannozzi, S. Baroni, N. Bonini, M. Calandra, R. Car, C. Cavazzoni, D. Ceresoli, G. L. Chiarotti, M. Cococcioni, I. Dabo, et al., *J. Phys.: Condens. Matter* **21**, 395502 (2009).
 - ³⁹ R. Sabatini, E. Küçükbenli, C. H. Pham, and S. de Gironcoli, *Phys. Rev. B* **93**, 235120 (2016).
 - ⁴⁰ A. M. Rappe, K. M. Rabe, E. Kaxiras, and J. D. Joannopoulos, *Phys. Rev. B* **41**, 1227 (1990).
 - ⁴¹ T. Böker, R. Severin, A. Müller, C. Janowitz, R. Manzke, D. Voß, P. Krüger, A. Mazur, and J. Pollmann, *Phys. Rev. B* **64**, 235305 (2001).
 - ⁴² O. Beckstein, J. E. Klepeis, G. L. W. Hart, and O. Pankratov, *Phys. Rev. B* **63**, 134112 (2001).
 - ⁴³ A. D. Corso, *J. Phys.: Condens. Matter* **28**, 075401 (2016).
 - ⁴⁴ H. Peelaers and C. G. VandeWalle, *Phys. Chem. Chem. Phys.* **118**, 12073 (2014).
 - ⁴⁵ J. Feldman, *J. Phys. Chem. Solids* **37**, 1141 (1976).
 - ⁴⁶ A. Togo and I. Tanaka, *Scr. Mater.* **108**, 1 (2015).